

Through-Space Charge Transfer and Nonlinear Optical Properties of Substituted Paracyclophane

Joseph Zyss,^{*,†} Isabelle Ledoux,[†] Sergei Volkov,[‡] Vladimir Chernyak,[‡] Shaul Mukamel,^{*,‡} Glenn P. Bartholomew,[§] and Guillermo C. Bazan^{*,§}

Contribution from the Laboratoire de Photonique Quantique et Moléculaire-UMR CNRS 8537, Ecole Normale Supérieure de Cachan, 61 avenue du Président Wilson, 94235 Cachan Cedex, France, Department of Chemistry, University of Rochester, Rochester, New York 14627, and Department of Chemistry and Materials, University of California, Santa Barbara, California 93106

Received June 22, 2000. Revised Manuscript Received September 15, 2000

Abstract: The introduction, within a π -conjugated donor–acceptor molecule, of an intermediate barrier to electron tunneling and its size scaling and influence on electronic polarization properties have remained so far elusive issues of great potential interest toward the fine-tuning of the linear and nonlinear optical properties of molecular materials. Paracyclophane (pCP) provides a most relevant cornerstone for more elaborate compounds where donor and acceptor substituents are made to interact through a sterically constrained π – π stack. A first attempt in this direction is reported here with the synthesis of a model dipolar 4-(4-dihexylaminostyryl)-16-(4-nitrostyryl)[2.2]paracyclophane and the subsequent experimental and theoretical study of its quadratic nonlinear optical properties. A major outcome of this investigation is the evidence of a significant “through-space” charge transfer as unambiguously designated by the strong departure of the β quadratic hyperpolarizability tensor of the full doubly substituted molecule (60×10^{-30} esu) from the additive β value (18×10^{-30} esu) expected for strictly noninteracting singly substituted pCP moieties. This desired increase of nonlinear efficiency upon substitution is not offset by the usual red-shift of the absorption spectrum which generally curtails application perspectives in more common uninterrupted conjugated chains. The collective nonlinear polarization behavior involving the full end-to-end molecular structure is confirmed by theoretical calculations using the Collective Electron Oscillator (CEO) approach which furthermore indicates a significantly enhanced role of electron–hole pair delocalization in the higher order nonlinear response, compared to the linear polarizability or the static dipole moment.

Paracyclophanes: A New Molecular Engineering Strategy for NLO

Most classical molecular engineering schemes underlying the design and the optimization of efficient molecules for quadratic nonlinear optical (NLO) applications are based on intramolecular charge transfer (ICT) processes from a donor toward an acceptor moiety through a π -electron conjugated path, such as in benzene, stilbene, azobenzene, polyene, or thiophene derivatives.^{1,2} Significant progress recently has been made in finding an adequate compromise between aromaticity and thermal stability of highly conjugated dyes in electrooptic and other device applications.³

In parallel with this mainstream line of research, nonconventional ICT schemes, such as “through-space” electronic interactions between donor and acceptor groups, have received more limited attention. From a more general perspective, noncovalent interactions are key factors in the field of molecular recognition.⁴ Among them, arene–arene interactions play an important role in the selective complexation of π -neutral guests

inside cyclophane moieties and molecular clefts.^{5,6} Such π – π electronic interactions could be advantageously involved in ICT processes underlying quadratic nonlinear properties at the molecular level: full or partial elimination of the conjugated electronic path may entail specific advantages such as favorable displacement of the nonlinearity/transparency tradeoff or a possible improvement of the thermal stability. However, evidence of the NLO implications of donor–acceptor ICT schemes through aryl–aryl “through-space” coupling is still scarce and somewhat inconclusive. As an example, functionalized 1,8-diarylnaphthalenes have been investigated,⁷ but the 2-dimensional character of the ICT was not addressed, thus weakening the assumption of inter-ring interactions.

The paracyclophane molecular template can be used as the cornerstone of a new strategy for acceptor–donor charge-transfer mediated and controlled by π – π stacking within the cyclophane moiety. In contrast with the full end-to-end π conjugation of usual polyene oligomers, such a “transmitter” chain can be viewed as a biased double potential well separated by a tunneling barrier. The donor–acceptor potential provides the bias, promoting directional charge transfer and the ensuing polar electronic displacement through the barrier.

* Address correspondence to these authors.

† Ecole Normale Supérieure de Cachan.

‡ University of Rochester.

§ University of California.

(1) *Molecular Nonlinear Optics: Materials, Physics and Devices*; Zyss, J., Ed.; Academic Press: Boston, 1994; p 129.

(2) Cheng, L.-T.; Tam, W.; Stevenson, S. H.; Meredith, G.; Rikken, G.; Marder, S. R. *J. Phys. Chem.* **1991**, *95*, 10631.

(3) Jen, A. K. Y.; Rao, V. P.; Drost, K. J.; Wong, K. Y.; Cava, M. P. *J. Chem. Soc. Chem. Commun.* **1994**, *1994*, 2057.

(4) Lehn, J.-M. *Angew. Chem., Int. Ed. Engl.* **1990**, *29*, 1304.

(5) Diederich, F. *Angew. Chem., Int. Ed. Engl.* **1988**, *27*, 362.

(6) Cozzi, F.; Cinquini, M.; Annunziata, R.; Siegel, J. S. *J. Am. Chem. Soc.* **1993**, *115*, 5330.

(7) Bahl, A.; Grahm, W.; Stadler, S.; Feiner, F.; Bourhill, G.; Bräuchle, C.; Reisner, A.; Jones, P. G. *Angew. Chem., Int. Ed. Engl.* **1995**, *34*, 1485.

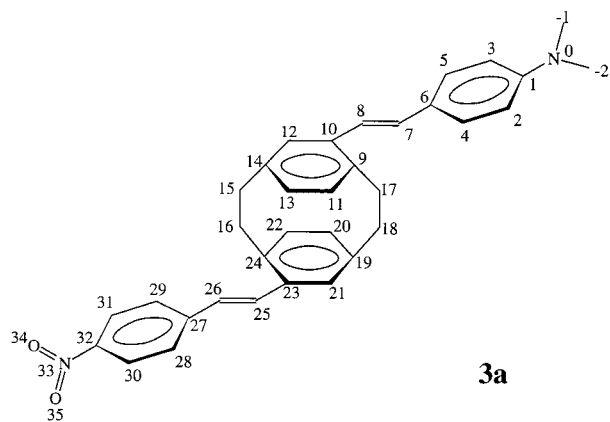


Figure 1. Atom numbering of **3a**. This simplified model of **3** was used in all computations.

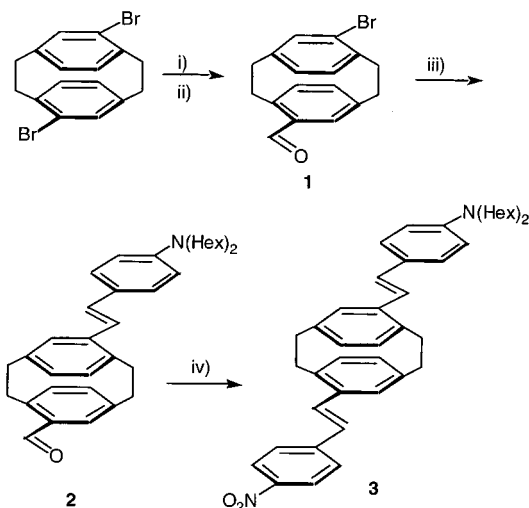
Paracyclophane (pCP) derivatives are therefore adequate templates for clear and unambiguous NLO experimental and theoretical studies of through-space electronic interactions. The two $\text{CH}_2\text{-CH}_2$ sp^3 1–1' and 4–4' lateral vertical linkages keeping the two phenyl groups in a bimolecular stack ensure the equivalence of the two attachment sites on the two aryl moieties, contrary to the case of 1,8-diarylnaphthyl derivatives, where the phenyl rings are linked together on one side only to the highly conjugated naphthyl moiety. This asymmetry fails to ensure that both rings remain parallel and results in a larger inter-aryl distance (~ 2.9 Å)⁷ than in the parallel benzene rings of the paracyclophane framework, where the mean inter-ring distance is ~ 2.6 Å. Moreover, the sp^3 -hybridized linkages between the two benzene rings screen the pCP transmitter core from electron-rich conjugated moieties that could otherwise disrupt the through-space ICT.

To clearly demonstrate, both theoretically and experimentally, the effects of inter-ring ICT between an electron donor grafted, for example, on the “lower” cycle of pCP and an electron acceptor group grafted to the “higher” cycle in the quasi-*para* position with respect to the donor (Figure 1), we have designed and synthesized the “model” compound 4-(4-dihexylaminostyryl)-16-(4-nitrostyryl)[2.2]paracyclophane. From synthetic considerations, a close equivalent of the paranitroaniline template happens to be a pCP-type molecule whereby two monosubstituted stilbenyl derivatives are attached sideways to form a staircase-like geometry. The present work concentrates on the demonstration of a purely “through-space” 1D ICT process in this model molecule. In section II we report and discuss the experimental results on synthesis and linear and nonlinear optical properties of the pCP molecule. In section III we report the calculation and analysis of the quadratic NLO response. Perspectives and future work are outlined in the conclusion.

Experimental Results

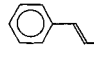
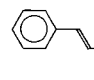
1. Synthesis. Consideration of the effect of molecular structure on expected nonlinear properties led us to choose as a synthetic target a pCP fragment that brings together a pair of stilbenoid units with donor and acceptor fragments (i.e. compound **3**). The requisite synthesis requires a nonstatistical functionalization of the pCP core.^{8,9} Our approach is shown in

Scheme 1^a



^a Conditions: (i) 1 equiv of *n*-BuLi in THF, -78 °C; (ii) 8 equiv of DMF; (iii) 4-dihexylaminostyrene, *P*(*o*-Tol)₃, Pd(OAc)₂, TEA, in DMF, 100 °C; (iv) (EtO)₂P(O)CH₂(4-NO₂-C₆H₄), NaOEt, THF, 0 °C.

Table 1. Dipole Moments μ , Maximum Absorption Wavelengths λ_{max} , Hyperpolarizability $\beta(\lambda)$, Static Hyperpolarizability $\beta(0)$, and “Additive” $\beta(0)$ of Donor- and Acceptor-Monosubstituted Stilbenes and of the PCP Molecule

Molecule	μ (D)		λ_{max} (nm)	$\beta(\lambda)$ (10^{-30} esu)	$\beta(0)$ (10^{-30} esu)		β_{add} (10^{-30} esu)	
	calc	exp			calc	exp	calc	exp
 <i>p</i> -dimethylaminostilbene ²	1.3	2.1	320	10 ($\lambda = 1.91 \mu\text{m}$) ²	7	9		
 <i>p</i> -nitrostilbene ²	6.8	4.2	345	11 ($\lambda = 1.91 \mu\text{m}$) ²	16	9		
3a	8.1	6.9	378	138 ($\lambda = 1.06 \mu\text{m}$)	38	60	23	18

Scheme 1. Monolithiation of 4,16-dibromo[2.2]paracyclophane¹⁰ followed by quenching with dimethylformamide affords compound **1** in 84% yield. Upon lithiation, the increased negative charge across the pCP bridge discourages a second deprotonation. The arylbromide functionality in compound **1** allows for functionalization by Heck coupling methodology using 4-dihexylaminostyrene. The resulting compound **2** is obtained in 65% yield after standard workup. The nitrostyryl functionality can be introduced subsequently by reaction of **2** with 4-nitrophenylmethanephosphonate. The target compound **3** is thus obtained in 74% yield.

Experimental results are summarized and reported in Table 1. The dipole moment and the hyperpolarizability of the pCP are compared to the sum of the corresponding values of the monosubstituted stilbene subunits, i.e., *p*-nitrostilbene (acceptor moiety) and *p*-(dimethylamino)stilbene (donor moiety)².

2. Dipole Moment. The dipole moment of our pCP molecule (Figure 1) is (6.9 ± 0.02) D in chloroform. As compared to the μ_{add} value from an additive model, whereby the dipole moments of individual *p*-nitrostilbene ($\mu_{\text{A}} = 4.2$ D) and of *p*-(dimethylamino)stilbene ($\mu_{\text{D}} = 2.1$ D) moieties are simply added ($\mu_{\text{add}} = 6.3$ D), the experimental μ value is found to be slightly higher than μ_{add} . This difference is marginal and cannot be viewed as an unambiguous experimental demonstration of ICT through the two benzene rings.

(8) Oldham, W. J., Jr.; Miao, Y.-J.; Lachicotte, R. J.; Bazan, G. C. *J. Am. Chem. Soc.* **1998**, *120*, 419.

(9) Bazan, G. C.; Oldham, W. J., Jr.; Lachicotte, R. J.; Tretiak, S.; Chernyak, V.; Mukamel, S. *J. Am. Chem. Soc.* **1998**, *120*, 9188. Wang, S.; Bazan, G. C.; Tretiak, S.; Mukamel, S. *J. Am. Chem. Soc.* **2000**, *122*, 1289.

(10) Reich, H. J.; Cram, D. J. *J. Am. Chem. Soc.* **1969**, *91*, 3527.

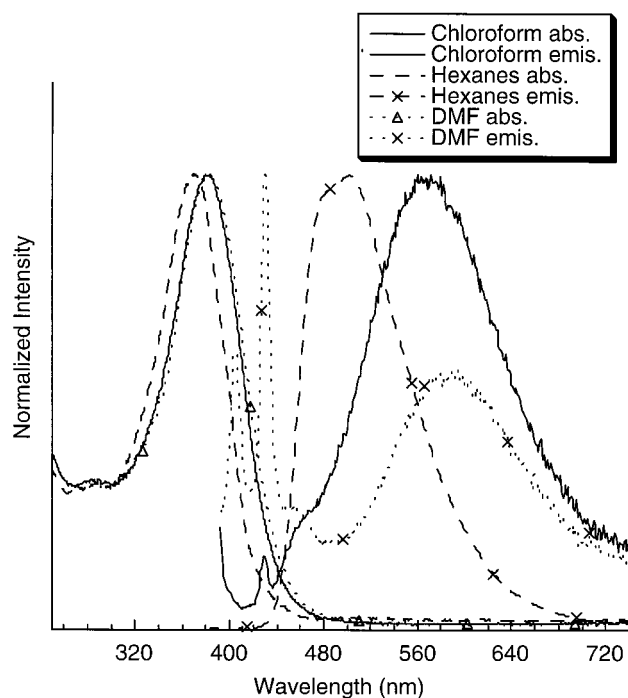


Figure 2. Absorption and emission spectra of **3** in various solvents.

Table 2. Absorbance and Fluorescence Data and Photoluminescence (PL) Quantum Yields for pCP in Several Organic Solvents

solvent	absorbance max (nm)	emission max (nm)	PL quantum efficiency
hexane	372	505	0.27
cyclohexane	374	509	0.36
diethyl ether	373	-	-
benzene	380	597	0.012
tetrahydrofuran	380	-	-
chloroform	383	570	0.002
<i>N,N</i> -dimethylformamide	384	590	<0.001

3. Absorption and Emission Spectra. The maximum absorption wavelength λ_{\max} of **3** is 378 nm in chloroform and is weakly sensitive to solvent polarity, as displayed in Figure 2. As reported in Table 2, the emission is centered around 500 nm in hexane and is strongly red-shifted to approximately 590 nm in more polar solvents such as chloroform and DMF, with a simultaneous fluorescence quenching at longer wavelengths and a strong spectral narrowing around 440 nm for DMF. Such significant emission red-shift indicates stronger sensitivity of the excited-state electronic distribution to environmental factors compared with the ground state. These solvent polarity effects suggest the possibility of an ICT between the donor and the acceptor groups.¹¹ Moreover, this molecule could be an interesting candidate for luminescence applications

4. Hyperpolarizability. The hyperpolarizability $\beta_{\text{EFISH}} = \beta_{\text{xxx}} + \beta_{\text{yyy}} + \beta_{\text{zzz}}$ of **3** was measured in CHCl_3 solution at 1.064 μm and the β_{EFISH} of the corresponding monosubstituted donor and acceptor subunits were measured at 1.9 μm . The optical properties of these molecules can be accounted for in terms of a two-level frequency dispersion model, applicable in the case of quasi-one-dimensional electronic polarization properties.¹² Static $\beta_{\text{EFISH}}(0)$ values can then be inferred from the experi-

mental $\beta_{\text{EFISH}}(\omega)$ data according to the following classical off-resonance expression:¹³

$$\beta_{\text{EFISH}}(\omega) = \beta_{\text{EFISH}}(0) \frac{W^4}{[W^2 - (\hbar\omega)^2][W^2 - (2\hbar\omega)^2]}$$

where W is the energy of the ICT transition and ω is the fundamental frequency.

The $\beta_{\text{EFISH}}(0)$ static value for **3** is found to be more than 3 times higher than β_{add} resulting from the parallel polar superposition of the two monosubstituted stilbene subunits. Such a large enhancement is a clear signature of the contribution of “through-space” charge transfer between the two pCP phenyl rings. As expected, β -related properties are much more sensitive indicators of ICT than dipole moments or linear polarizability properties.¹⁴ Moreover, $\beta_{\text{EFISH}}(0)$ and $\mu \cdot \beta_{\text{EFISH}}(0)$ values are close to those of the Disperse Red 1 (DR1)¹⁵ molecule, with the additional advantage of a broader transparency range in **3**. It appears that tunneling through the pCP central moiety maintains transparency while ensuring strong through-space charge-transfer contribution to β as evidenced by the large departure from additivity.

Calculation of the Off-Resonance Quadratic Optical Response

We have applied the collective electronic oscillator (CEO) approach^{16–18} to compute the off-resonant second-order electronic polarizability β of the para-substituted pCP molecule **3a** as well as the contributions from separate atoms to this quadratic response. The CEO computes the reduced single-electron density matrix ρ_{mn} ^{19,20} using the time-dependent Hartree–Fock (TDHF) procedure. The matrix elements ρ_{mn} are defined as the expectation values of the operators $\hat{c}_m^+ \hat{c}_n$, where $\hat{c}_n^+ (\hat{c}_n)$ are the creation (annihilation) operators of an electron in the n th atomic orbital. Given ρ_{mn} , one can calculate the expectation value of any one-electron operator, such as the dipole moment, and avoid the time-consuming and unnecessary computation of the full many-electron wave function, making the approach an attractive low-cost tool for computing molecular polarizabilities.

We have used the optimal ground-state geometry calculated at the AM1 level with Gaussian-98.²¹ Different parts of our code were described in refs 17 and 22. It makes use of the ZINDO program^{23,24} to produce the INDO/S Hamiltonian and the dipole operator in the atomic orbitals basis set. Each hydrogen is assigned a single s-type basis function, while each carbon or other heavy atom has one s- and three p-type atomic orbitals

(13) Oudar, J.-L. *J. Chem. Phys.* **1977**, *67*, 446.

(14) Zyss, J. *J. Chem. Phys.* **1979**, *71*, 909.

(15) Singer, K. D.; Kuzyk, M. G.; Sohn, J. E. *J. Opt. Soc. Am. B* **1987**, *4*, 968.

(16) Tretiak, S.; Chernyak, V.; Mukamel, S. *Chem. Phys. Lett.* **1996**, *259*, 55. Tretiak, S.; Chernyak, V.; Mukamel, S. *J. Chem. Phys.* **1996**, *105*, 8914.

(17) Tretiak, S.; Chernyak, V.; Mukamel, S. *J. Am. Chem. Soc.* **1997**, *119*, 11408. Tretiak, S.; Chernyak, V.; Mukamel, S. *Chem. Phys. Lett.* **1998**, *287*, 75.

(18) Mukamel, S.; Tretiak, S.; Wagersreiter, T.; Chernyak, V. *Science* **1997**, *277*, 781. Mukamel, S.; Takahashi, A.; Wang, H. X.; Chen, G. *Science* **1994**, *266*, 250.

(19) McWeeny, R.; Sutcliffe, B. T. *Methods of Molecular Quantum Mechanics*; Academic Press: New York, 1976.

(20) Davidson, E. R. *Reduced Density Matrixes in Quantum Chemistry*; Academic Press: New York, 1976.

(21) Frisch M. J. et al., GAUSSIAN 98; Gaussian: Pittsburgh, 1999.

(22) Chernyak, V.; Schulz, M.; Mukamel, S.; Tretiak, S.; Tsiper, E. *J. Chem. Phys.* **2000**, *113*, 36.

(23) Ridley, J.; Zerner, M. C. *Theor. Chim. Acta* **1973**, *32*, 111.

(24) Zerner, M. C.; Loew, C. H.; Kirchner, R. F.; Mueller-Westerhoff, U. T. *J. Am. Chem. Soc.* **1980**, *102*, 589.

(11) McRae, E. G. *J. Phys. Chem.* **1957**, *61*, 562.

(12) Brasselet, S.; Zyss, J. *J. Nonlinear Opt. Phys. Mater.* **1996**, *4* (No. 4), 671–693.

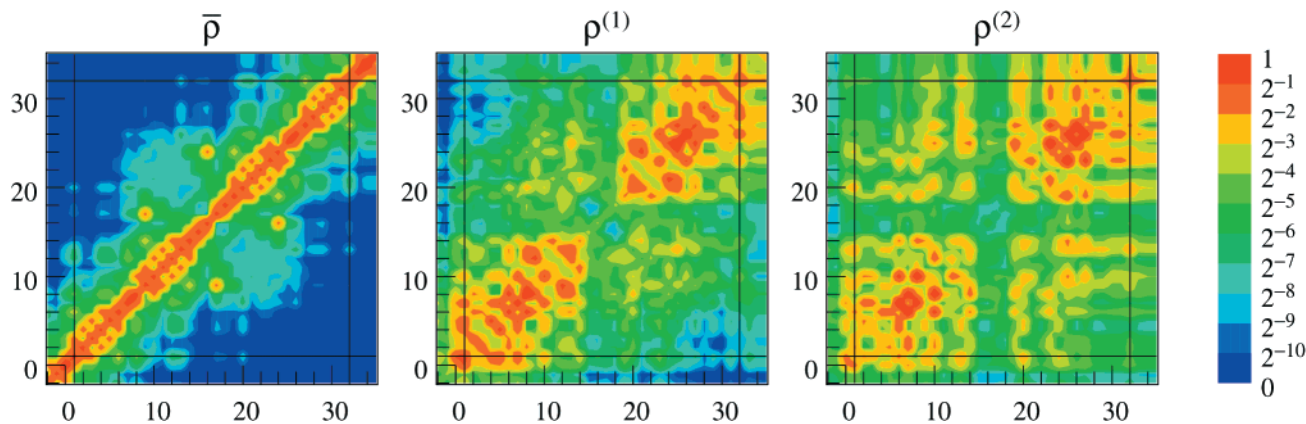


Figure 3. Contour plot (logarithmic scale) representing the ground-state density matrix $\bar{\rho}_{mn}$ and the induced density matrices $\rho_{mn,x}^{(1)}$ and $\rho_{mn,xx}^{(2)}$.

(we only consider closed-shell configurations where spin variables can be excluded and the electrons are counted in pairs). First, the ground-state reduced single-electron density matrix $\bar{\rho}_{mn}$ is found within the Hartree–Fock approximation. The program then calculates the electronic normal modes (transition single-electron density matrices driven by the external electric field) as described in ref 17. The 50 lowest energy eigenmodes of the linearized TDHF equations of motion for the density matrix were computed by using the oblique Lanczos algorithm.²² The induced static single-electron density matrix was then expanded in these electronic modes (see ref 17 for details). To test convergence we have also employed the density-matrix-spectral-moment algorithm (DSMA)¹⁶ which calculates a smaller number (about 15) of dominating electronic modes for the molecular response. These electronic oscillators do not reveal a very detailed structure of the electronic spectrum, but give a good low-resolution approximation, covering a much broader frequency region than the oblique Lanczos algorithm. Our DSMA calculations have shown that the electronic modes from the frequency region above the highest electronic oscillator frequency found with the Lanczos algorithm (≥ 6 eV) make only a negligible contribution to β . The β values found with these two methods only differ by a few percent.

To compute the optical response, the reduced single-electron density matrix ρ_{mn} is expanded in powers of the static external field E_i :

$$\rho_{mn} = \bar{\rho}_{mn} + \rho_{mn,i}^{(1)}E_i + \rho_{mn,ij}^{(2)}E_iE_j \quad (1)$$

where i, j denote the Cartesian coordinates and summation is performed over repeated indices. The induced dipole moment to quadratic order in the external field is given by:

$$P_i^{(2)} = \beta_{ijk}E_jE_k \quad (2)$$

The off-resonance quadratic polarizability of the molecule β_{ijk} is expressed through $\rho_{mn,ij}^{(2)}$ and the dipole-moment matrix elements $\mu_{mn,i}$:

$$\beta_{ijk} = \sum_{mn} \mu_{mn,i} \rho_{mn,jk}^{(2)} \quad (3)$$

x directed along the molecular axis from the donor to the acceptor. Hence, the most interesting tensor component of the quadratic polarizability of the molecule is the diagonal β_{xxx} , which is much larger than the nondiagonal terms β_{xyy} and β_{xzz} that contribute to the experimental EFISH value $\beta_{\text{EFISH}} = \beta_{xxx} + \beta_{xyy} + \beta_{xzz}$. Our calculations give $|\beta_{xxx}| = 38 \times 10^{-30}$ esu, which is in reasonably good agreement with the experimental

value of 60×10^{-30} esu, and the difference can be attributed to the solvent effects which are not accounted for in these computations.

The off-diagonal elements of the ground-state density matrix $\bar{\rho}_{mn}$ represent the quantum-mechanical correlations between the m th and the n th atomic orbitals. The diagonal elements $\bar{\rho}_{mn}$ give the net charges on a particular n th orbital. The elements of the induced matrices $\rho_{mn,i}^{(1)}$, $\rho_{mn,jk}^{(2)}$ represent the corrections to these correlations or charges to first and second order in the incoming fields, respectively. To display the correlations among atoms we have summed all the contributions to the density matrix from the orbitals residing on each atom and consider the resulting effective density matrices $\bar{\rho}_{aa'}$.

$$\bar{\rho}_{aa'}^2 = \sum_{\substack{m:A(m)=a \\ n:A(n)=a'}} (\bar{\rho}_{mn})^2 \quad (4)$$

The indices a, a' now run over the atoms and not the atomic orbitals and the coarse grained density matrix $\bar{\rho}_{aa'}$ represents the charges and effective coherences between the various atoms. $\rho_{aa',i}^{(1)}$, $\rho_{aa',jk}^{(2)}$ are defined in a similar way. The contour plots in Figure 3 show the ground-state density matrix $\bar{\rho}_{aa'}$ and the induced density matrices $\rho_{aa',x}^{(1)}$ and $\rho_{aa',xx}^{(2)}$ where the axes are labeled by the atoms.

The numbering of the heavy atoms in **3a** starts from its “donor” side, with the heavy atoms in the $\text{N}(\text{CH}_3)_2$ donor group itself having labels $a < 1$ (see Figure 1); the hydrogen atom contributions are not shown. $\bar{\rho}_{aa'}$, $\rho_{aa',x}^{(1)}$ and $\rho_{aa',xx}^{(2)}$ are normalized to their respective maxima and plotted on a logarithmic scale. The color code represents the relative value of the elements of the effective density matrix describing the quantum-mechanical correlation between a given pair of atoms. The color code spans 3 orders of magnitude from blue (small) to red (large). The solid lines in the plots mark the first and the last atoms of the “bridge” between the donor and the acceptor regions. The plots clearly show that the ground-state density matrix has very small cross-terms (off-diagonal blocks) with an electron on one part of the molecule and a hole on the other part, and that the coherences between two parts increase with the order of nonlinear response. We characterize the relative weight of these cross-terms by the quantity R_X^2 defined as the ratio of the mean square of all matrix elements representing the electron and hole on different halves of the molecule (off-diagonal blocks) to those representing the electron and hole on the same half of the molecule (diagonal blocks). R_X is 0.12 for $\bar{\rho}_{aa'}$, 0.18 for $\rho_{aa',x}^{(1)}$ and 0.36 for $\rho_{aa',xx}^{(2)}$, the fact that R_X is found to be three times larger for the second-order response compared

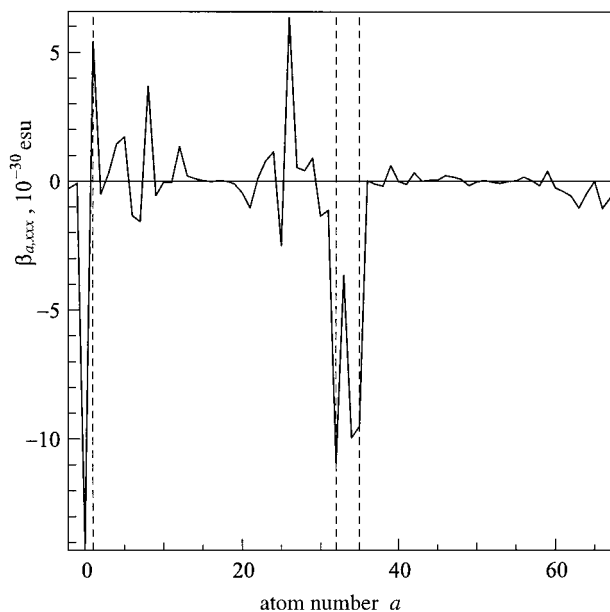


Figure 4. Contributions of different atoms of **3a** to its off-resonance quadratic polarizability component β_{xxx} .

with the ground state supporting the experimental observations of the additivity of μ and the nonadditivity of β .

Our calculations show that the main contributions to eq 3 come from the diagonal and near-diagonal matrix elements of $\mu_{mn,i}$ and $\rho_{mn,ij}^{(2)}$ where the m th and n th atomic orbitals belong to the same atom. This allowed us to approximately decompose the polarizability tensor β into contributions from different atoms, so that

$$\beta_{ijk} = \sum_a \tilde{\beta}_{a,ijk} \quad (5)$$

where

$$\tilde{\beta}_{a,ijk} = \sum_{\substack{m:A(m)=a \\ n:A(n)=a}} \mu_{mn,i} \rho_{nm,jk}^{(2)} \quad (6)$$

Here the index a refers to the atoms, and $A(n)$ is the atom label to which the n th atomic orbital belongs. When decomposing β_{ijk} in this way, one should note that the dipole moments of individual atoms generally depend on the choice of origin, since a net charge resides on each atom. The total dipole moment of the molecule is nevertheless independent of the choice of the origin, because the molecule is electrically neutral. In the following, we set the origin of the dipole moments of all the atoms at the center of mass of the molecule.

The following real-space analysis of the nonlinear response follows naturally from the CEO calculation and allows us to trace the microscopic origin of β . Figure 4 shows the contributions to β_{xxx} from different atoms, $\tilde{\beta}_{a,xxx}$. We notice four regions, separated by the dashed lines: the donor region (atoms $-1, -2, 0$), the centrosymmetric bridge connecting the donor and the acceptor (atoms 1 through 32), the acceptor heavy atoms (33, 34, 35), and finally the hydrogen atoms (36 through 67) in no particular order.

Because of the inversion symmetry of the bridge its total contribution to β in the absence of the donor and the acceptor should vanish, and the dependence of $\tilde{\beta}_{a,xxx}$ on a should be antisymmetric (i.e. the contributions from any symmetric pair of atoms in such a truncated molecule should be of opposite sign but of the same absolute value). This was verified by our

Table 3. The Largest Contributions from Different Atoms to the Off-Resonance Quadratic Polarizability of **3a** Molecule

type of atom	no. of atoms	contribution to β_{xxx} (10^{-30} esu)	cumulative β_{xxx} (10^{-30} esu)
N	0	-14.1	-14.1
C	32	-10.9	-25.0
O	34	-10.0	-35.0
O	35	-9.5	-44.5
C	26	6.3	-38.1
C	1	5.4	-32.7
C	8	3.7	-29.0
N	33	-3.6	-32.7
H	(all)	-3.2	-35.9
C	25	-2.5	-38.4
C	5	1.7	-36.7
C	7	-1.6	-38.3
C	4	1.4	-36.8
C	30	-1.4	-38.2
C	12	1.3	-36.8
C	6	-1.3	-38.2
C	24	1.1	-37.0
C	31	-1.1	-38.2
C	21	-1.0	-39.2
C	29	0.9	-38.3
total β_{xxx}			-37.9

calculations for a symmetric bridge (not shown). Figure 4 illustrates that this symmetry is broken by the substitutions, and the most noticeable distortions are found in the vicinities of the donor and the acceptor.

The contributions to Figure 4 are given in Table 3 where we have arranged the largest contributions to β_{xxx} from different atoms in descending order of their absolute values. The strongest contributions come from the donor and acceptor groups, and they have the same sign, as opposed to the asymmetric contributions from the carbons in the central part of the bridge. The hydrogen atoms make a small contribution, and we only give their total contribution. The last column illustrates the convergence of the cumulative sum of the strongest contributions to β_{xxx} to the total β_{xxx} of the molecule.

Conclusions

The search for an optimal transparency–efficiency tradeoff for optically nonlinear molecules has been a constant motivation for molecular engineering studies over almost two decades. Whereas the electron donor or acceptor ends provide interesting degrees of freedom, their intermediary polarization transmitting linkage may follow other patterns than that of the traditional single and double bond alternation of polyene-like conjugated chains. We have proposed and demonstrated here such an alternative structure whereby the intermediary linkage contains an “obstacle” in the form of a π – π stack as from the central paracyclophane moiety. Gross nonadditivity of the experimental β of an asymmetrically donor–acceptor substituted pCP, shown by EFISH measurements, suggests a significant end-to-end charge-transfer contribution to the quadratic nonlinear polarizability. This is substantiated further by quantum chemical calculations based on the collective electronic oscillator approach, demonstrating strong involvement of charge delocalization to the dominant β tensor coefficient.

Using a possibly oversimplified, however striking analogy with a semiconductor structure, such a molecule can be viewed in many ways as a one-dimensional biased heterojunction where two electron-rich potential wells are connected through a junction acting as a barrier, as shown in Figure 5. The central pCP building block provides a synthetically versatile promising starting point for extending the preliminary results from this

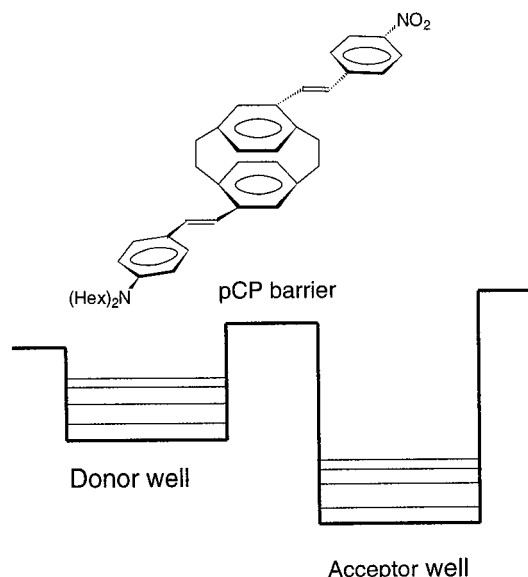


Figure 5. Analogy between a model heterojunction and the polar-substituted donor-acceptor pCP.

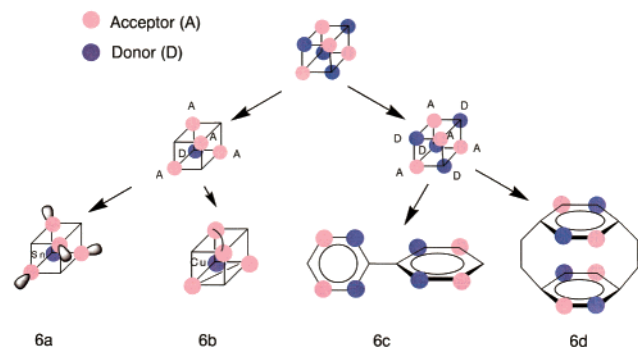


Figure 6. Various strategies for engineering of octupolar 3D molecules: centered tetrahedral covalent Sn derivative (**6a**),³³ Cu^{II}-bis-bipyridine complex (**6b**),³⁴ fully tetrahedral purely organic biphenyl (**6c**),³⁵ and pCP (**6d**).

study. In particular, it has been demonstrated over the last years that the donor-acceptor dipolar molecular paranitroaniline template, based on a single pair of donor and acceptor substituents, can be successfully generalized to multiple charge-transfer interactions such as in “multipolar structures”.²⁵ More general 3D molecular engineering schemes for quadratic NLO deriving from the same cubic point charge template²⁶ can be indeed implemented into various synthetic strategies involving organometallic molecules, biphenyls, and others as summarized in Figure 6.

On the basis of the substitutional potential of the pCP at different carbon sites, we are currently extending this work to octupolar and more generally multipolar pCP based units as well as to other third-order or two-photon absorption properties, where multidimensional through-space tunneling is expected to play an important role.

Experimental Section

General Details. All synthetic manipulations were performed under an inert atmosphere in a nitrogen-filled glovebox and using Schlenk techniques. All reagents were obtained from Aldrich and were used as received. ¹H NMR and ¹³C NMR spectra were obtained on a Varian Unity 400 MHz spectrometer. High-resolution mass spectra were

performed on a VG-70SE double-focusing system using electron ionization. 4-Dihexylaminostyrene²⁷ and diethyl 4-nitrophenylmethane-phosphonate²⁸ were obtained by procedures described earlier. All solvents used for reactions were dried by stirring with Na metal overnight followed by degassing and vacuum transfer.

4-Bromo-16-carboxaldehyde-[2.2]paracyclophane (1). A 1 L 24/40 round-bottom flask was charged with a magnetic stirbar and 4,16-dibromo[2.2]paracyclophane¹⁰ (2.306 g, 6.3 mmol). Approximately 450 mL of dry THF was vacuum transferred into the reaction flask. The reaction mixture was cooled to -78°C and 4 mL of *n*-BuLi (1.6 M, 6.3 mmol) was added via syringe. The solution became orange in color and faded. This step was allowed to proceed for 30 min. Anhydrous DMF (4 mL, 8 equiv) was added all at once, and the mixture was stirred vigorously and allowed to warm slowly to room temperature. After the mixture was quenched with a dilute solution of NH₄OH, THF was removed under vacuum. The resulting solid was diluted in CHCl₃ (ca. 350 mL) and washed three times with deionized water and then dried over MgSO₄. Recrystallization with hot EtOH yielded 1.85 g of off-white crystals. Subsequent recrystallizations from CHCl₃/hexane (1:3) afforded 1.67 g, for a yield of 84%. ¹H NMR (CDCl₃) δ 9.964 (s, 1H), 7.415 (dd, 1H), 6.985 (d, 1H), 6.561 (m, 2H), 6.6423 (m, 2H), 4.127 (m, 1H), 3.506 (m, 1H), 3.25–2.84 (multiplets, 6H). ¹³C NMR (CDCl₃) 192.304, 142.915, 141.655, 140.297, 139.121, 137.384, 137.217, 136.739, 135.343, 134.221, 133.932, 130.882, 127.537, 35.344, 34.320, 33.326, 33.122. HRMS-EI *m/z* 314.0305, $\Delta = 0.6$ ppm.

4-Carboxaldehyde 16-(4'-Dihexylaminostyryl)[2.2]paracyclophane (2). A 50 mL 24/40 round-bottom flask equipped with a Teflon-coated magnetic stirbar was charged with 1-bromoparacyclophane-4'-al (552 mg, 1.75 mmol), 4-dihexylaminostyrene (502 mg, 1.75 mmol), Pd(OAc)₂ (30 mg), tris(*o*-tolyl)phosphine (304 mg, 1 mmol), and 1 mL of triethylamine. DMF (10 mL) was added via syringe and the flask was heated to 100°C for 24 h. The mixture was diluted in CHCl₃, washed three times with deionized water, and then dried over MgSO₄. The solvent was removed under vacuum and the resulting oily liquid was purified by flash chromatography (90 g silica column, 40% hexanes in CHCl₃). The product was a yellow-orange solid (594 mg, 65% yield). ¹H NMR (CDCl₃) δ 9.978 (s, 1H), 7.460 (d, 2H), 6.996 (dd, 2H), 6.934 (d, 1H), 6.807 (d, 1H), 6.680 (dd, 2H), 6.637 (d, 1H), 6.521 (d, 1H), 6.387 (d, 1H), 6.339 (dd, 1H), 4.125 (m, 1H), 3.593 (m, 1H), 3.319 (t, 4H), 3.26–2.85 (multiplets, 6H), 1.625 (m, 4H), 1.36 (m, 12H), 0.930 (m, 6H). ¹³C NMR (CDCl₃) 192.349, 148.066, 143.271, 140.366, 139.660, 138.864, 137.665, 136.853, 136.580, 134.736, 134.001, 130.222, 130.184, 129.600, 128.015, 124.866, 121.824, 111.810, 51.307, 34.836, 34.229, 33.524, 33.159, 31.946, 27.477, 27.045, 22.902, 14.276. HRMS-EI *m/z* 521.3664, $\Delta = 1.3$ ppm.

4-(4'-Dihexylaminostyryl)-16-(4'-nitrostyryl)-[2.2]paracyclophane (3). A 50 mL 24/40 round-bottom flask equipped with a Teflon-coated magnetic stirbar was charged with 4-carboxaldehyde-16-(4'-dihexylaminostyryl)[2.2]paracyclophane (261 mg, 0.5 mmol), 4-nitrophenylmethane-phosphonate (164 mg, 0.6 mmol), and approximately 3 mL of anhydrous DMF. The reaction mixture was cooled to 0°C and NaOEt (ca. 60 mg) was added. The reaction was allowed to warm to room temperature and proceeded for 12 h. The reaction was quenched with deionized water, transferred and then diluted (ca. 500 mL) with CHCl₃, washed three times with deionized water, and then dried over MgSO₄. After filtration, the solvent was removed and an oily liquid resulted. This mixture was subsequently separated on a 90 g flash chromatography column with 40% hexanes in CHCl₃ as the eluent. After removal of solvent by rotary evaporation, 237 mg (74% yield) of a bright yellow solid was collected. ¹H NMR (CDCl₃) δ 8.273 (m, 2H, H_q), 7.693 (m, 2H, H_p), 7.463 (d, 2H, H_c), 7.404 (d, 1H, H_o), 6.958 (dd, 2H, H_f and H_g), 6.819 (d, 1H, H_n), 6.778 (m, 1H, H_i or H_l), 6.690 (m, 1H, H_h or H_k), 6.528 (m, 1H, H_i or H_l), 6.444 (d, 1H, H_j or H_m), 6.385 (d, 1H, H_j or H_m), 3.608 (m, 2H, H_s and H_t), 3.319 (t, 4H, H_a), 3.19–2.85 (multiplets, 6H, H_r, H_{r'}, H_t, H_{t'}, H_u, and H_{u'}), 1.626 (m, 4H, H_b), 1.353 (m, 12H, H_v), 0.925 (t, 6H, H_c). ¹³C NMR (CDCl₃) 148.005, 146.807, 144.713, 140.085, 139.281, 139.243, 138.689, 137.718, 136.368, 133.970, 133.621, 131.816, 130.708,

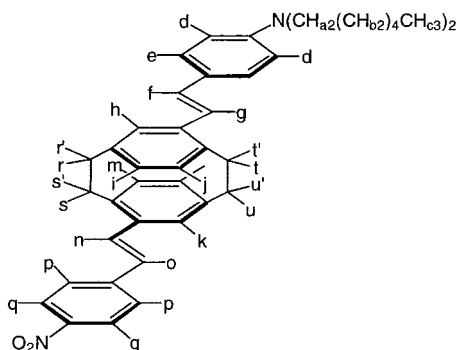
(25) Zyss, J. *Nonlinear Opt.* **1991**, *1*, 3.

(26) Zyss, J. *J. Chem. Phys.* **1993**, *98*, 6583.

(27) Oprea, S.; Still, R. H. *J. Appl. Polym. Sci.* **1976**, *20*, 639.

(28) Wadsworth, D. H.; Schupp, O. E.; Sees, E. J.; Ford, J. A., Jr. *J. Org. Chem.* **1964**, *30*, 680.

130.632, 129.980, 129.904, 128.773, 127.984, 126.983, 126.824, 125.086, 124.464, 122.105, 111.848, 51.345, 34.904, 34.502, 33.675, 33.531, 31.976, 27.515, 27.083, 22.933, 14.299. HRMS-EI m/z 640.4031, $\Delta = 0.3$ ppm.



Measurement of Dipole Moment. The dipole moment μ is determined using the standard method of Guggenheim,²⁹ where μ is related to the refractive index n (respectively n_0) and to the dielectric constant ϵ (respectively ϵ_0) of a chloroform solution (respectively of pure chloroform) at a molecular concentration c :

$$\mu^2 = \frac{9kT}{4\pi N} \frac{3}{(\epsilon_0 + 2)(n_0^2 + 2)} \left(\frac{(\epsilon - n^2) - (\epsilon_0 - n_1^2)}{c} \right)$$

μ^2 is taken as the limit when c becomes vanishingly small. Refractive indices are measured with an Abbe prism refractometer (Carl Zeiss), and dielectric constants are obtained from capacitance measurements of a cylindrical condensator at 1 MHz (WTW), calibrated with a set of pure liquids of known dielectric constants. The temperature is maintained constant at 25 °C and the relative experimental error does not exceed 2% on μ .

Linear Optical Measurements. UV–visible absorption was recorded on a Shimadzu UV-2401 PC diode array spectrophotometer and photoluminescence spectra on a Spex fluoromax-2 spectrometer in

(29) Guggenheim, E. A. *Trans. Faraday Soc.* **1949**, *45*, 203.

various solvents. Solutions were prepared in hexane, cyclohexane, diethyl ether, benzene, tetrahydrofuran, chloroform, and *N,N*-dimethylformamide and diluted so that the absorption maximum was approximately 0.1. All solutions were degassed prior to final absorbance and fluorescence measurements and transferred to 1 cm quartz cuvettes. Fluorescence was measured at right angles using 373 nm. The quantum yield was calculated from the relation:³⁰

$$\Phi_u = \Phi_s [A(\lambda)_s F_u n_u^2 / (A(\lambda)_u F_s n_s^2)]$$

where the subscripts *s* and *u* indicate the standard and unknown sample, $A(\lambda)$ corresponds to the absorbance of the solution at the exciting wavelength λ , F is the integrated luminescence spectrum, and n is the index of refraction for the solvent carrying the unknown and the standard at the sodium D line. The standard fluorophore for solution measurements was 9,10-diphenylanthracene³¹ with $\Phi_{PL} = 0.90$.

Nonlinear Optical Measurements. In view of the quasi 1D and strongly polar character of the quadratic hyperpolarizability β of the molecule, the Electric-Field-Induced Second Harmonic generation (EFISH)^{13,32} is performed in chloroform solutions, with increasing concentrations ranging from $(2 \times 6) \times 10^{-3}$ to $(1 \times 3) \times 10^{-2}$ mol·L⁻¹. The source is a Q-switched Nd³⁺:YAG laser operating at 1.064 μ m, delivering pulses of 10 ns duration at a 10 Hz repetition rate, with an energy of approximately 1 mJ per pulse. A high voltage (8 kV) and short duration (1.5 μ s) electric pulse, synchronized with the laser pulse, breaks the centrosymmetry of the liquid by dipolar orientation of the molecules. Calibrations are made with respect to the pure solvent. Relative experimental errors do not exceed 3%.

Acknowledgment. The support of the National Science Foundation and the Petroleum Research Fund, administered by the American Chemical Society, is gratefully acknowledged.

JA0022526

- (30) Eaton, D. F. *Pure Appl. Chem.* **1998**, *60* (7), 1107.
 (31) Hamai, S.; Hirayama, F. *J. Phys. Chem.* **1983**, *87*, 83.
 (32) Ledoux, I.; Zyss, J. *Chem. Phys.* **1982**, *73*, 203.
 (33) Lequan, M.; Branger, C.; Simon, J.; Thami, T.; Chauchard, E.; Persoons, A. *Chem. Phys. Lett.* **1994**, *229*, 101.
 (34) Renouard, T.; Le Bozec, H.; Brasselet, S.; Ledoux, I.; Zyss, J. *Chem. Commun.* **1999** 871.
 (35) Blanchard-Desce, M.; Baudin, J.-B.; Jullien, L.; Lorne, R.; Ruel, O.; Brasselet, S.; Zyss, J. *Opt. Mater.* **1999**, *12*, 333.